

The Synthesis, Characterization, and Structure Solution of SSZ-58: A Novel Two-Dimensional 10-Ring Pore Zeolite with Previously Unseen Double 5-Ring Subunits

Allen Burton,* Saleh Elomari,* Ronald C. Medrud, Ignatius Y. Chan, Cong-Yan Chen, Lucy M. Bull, and E. Steven Vittoratos

Contribution from the ChevronTexaco Energy Research and Technology Center, Richmond, California 94802

Received October 3, 2002; E-mail: buaw@chevrontexaco.com; selomari@chevrontexaco.com

Abstract: The synthesis, structure solution, and characterization of the novel zeolite SSZ-58 are described. SSZ-58 was synthesized under hydrothermal conditions using 1-butyl-1-cyclooctylpyrrolidinium cation as a structure-directing agent. The framework topology of SSZ-58 was determined with the FOCUS Fourier recycling method. SSZ-58 possesses 12 tetrahedral atoms in the asymmetric unit of its highest topological symmetry, and to date it is the most complex zeolite structure solved from powder data. Rietveld refinement of synchrotron powder X-ray diffraction data in space group *Pmma* confirmed the proposed model. SSZ-58 contains layers of atoms that are linked together by double five-membered rings (D5R), or 5²4⁵ subunits, that have not been observed before in any zeolite or zeotype structures. SSZ-58 possesses a two-dimensional channel system consisting of 10-membered ring pores that intersect to form large cavities circumscribed by 12- and 16-membered ring pores.

1. Introduction

Zeolites find widespread use as catalysts, adsorbents, and ion exchangers.¹ New zeolites continue to emerge at an increasingly rapid pace.² The syntheses of high-silica zeolites are usually performed hydrothermally in the presence of an organocationic structure-directing agent (SDA).³ The size and shape of the SDA often correlate well with the dimensions of the zeolite micropores or cages. An understanding of molecular recognition effects in zeolite synthesis begins with identification of the structure or structures promoted by certain SDAs. A detailed knowledge of zeolite structure is also crucial for understanding catalytic and adsorptive properties. Once the structure of a zeolite is determined, applications based upon size- or shape-selective processes may be targeted.

Although structure solutions of zeolites from single crystals have been reported,^{4,5} it is rare that synthetic zeolite crystals are large enough for single-crystal structure analyses of novel zeolite phases. Investigators must therefore rely on powder diffraction data. Ab initio structure solution from powder data is difficult because of the high degree of peak overlap inherent to most powder patterns. If the intensities of the overlapping

reflections could be unambiguously determined, then the same direct methods applied to single-crystal data could be readily applied to powder data. Indeed, zeolite structures with small unit cells or a small number of tetrahedral atoms in their asymmetric units can be solved from direct methods by simply equipartitioning overlapping intensities. Improved results can be obtained by dividing overlapping intensities with triplet or quartet relations⁶ or with the fast iterative Patterson squaring (FIPS) routine.^{7,8} However, an upper limit on the success of direct methods remains at approximately 6–8 tetrahedral (T) atoms per asymmetric unit.⁶

In the past, there was often a long time between the initial discovery of a zeolite and its structure elucidation. The investigators hoped to construct a model that was consistent with the unit cell parameters, the possible space group symmetries, and the physicochemical (e.g., adsorption, catalytic, and density) data. These structure solutions often depended on simple modifications of previously known zeolite topologies. Insertion of 4-membered ring units (σ expansions) as in the ZSM-48⁹/SSZ-31¹⁰/UTD-1¹¹ series of disordered zeolites or substitution of mirror planes for inversion centers¹² are common themes relating different zeolite topologies. Model building continues to be an important tool to the zeolite crystallographer. However,

- (1) (a) Breck, D. W. *Zeolite Molecular Sieves: Structure, Chemistry, and Use*; Wiley: New York, 1974. (b) Venuto, P. B. *Microporous Mater.* **1994**, *2*, 297.
- (2) Baerlocher, C.; Meier, W. M.; Olson, D. H. *Atlas of Zeolite Framework Types*, 5th ed; Elsevier: New York, 2001. Also available at <http://www.iza-structure.org>.
- (3) Lobo, R. F.; Zones, S. I.; Davis, M. E. *J. Inclusion Phenom. Mol. Recognit. Chem.* **1995**, *21*, 47.
- (4) Chen, C. Y.; Finger, L. W.; Medrud, R. C.; Crozier, P. A.; Chan, I. Y.; Harris, T. V.; Zones, S. I. *Chem. Commun.* **1997**, 1775.
- (5) Cambor, M. A.; Diaz-Caban, M. J.; Perez-Pariente, J.; Teat, S. J.; Clegg, W.; Shannon, I. J.; Lightfoot, P.; Wright, P. A.; Morris, R. E. *Angew. Chem., Int. Ed.* **1998**, *37*, 2122.

- (6) Jansen, J.; Peschar, R.; Schenk, H. *J. Appl. Crystallogr.* **1992**, *25*, 237.
- (7) Estermann, M. A.; Gramlich, V. *J. Appl. Crystallogr.* **1993**, *26*, 396.
- (8) Estermann, M. A.; McCusker, L. B.; Baerlocher, C. *J. Appl. Crystallogr.* **1992**, *25*, 539.
- (9) Schlenker, J. L.; Rohrbaugh, W. J.; Chu, P.; Valyocsik, E. W.; Kokotailo, G. T. *Zeolites* **1985**, *5*, 355.
- (10) Lobo, R. F.; Tsapatsis, M.; Freyhardt, C. C.; Chan, I.; Chen, C. Y.; Zones, S. I.; Davis, M. E. *J. Am. Chem. Soc.* **1997**, *119*, 3732.
- (11) Lobo, R. F.; Tsapatsis, M.; Freyhardt, C. C.; Khodabandeh, S.; Wagner, P.; Chen, C. Y.; Balkus, K. J.; Zones, S. I.; Davis, M. E. *J. Am. Chem. Soc.* **1997**, *119*, 8474.

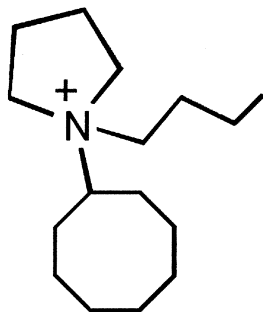


Figure 1. 1-Butyl-1-cyclooctylpyrrolidinium cation used as a structure-directing agent for the synthesis of SSZ-58.

if an unsolved structure contains previously unobserved secondary building units and especially if it possesses a large number of tetrahedral (T) atoms in its asymmetric unit, then the success of model building is more dubious.

Recently with the advent of the FOCUS^{13,14} and ZEFSAII¹⁵ algorithms, there have been significant advances in ab initio structure solution of zeolites from powder diffraction data. These methods incorporate the crystal chemical information inherent to most zeotype structures: that is, a fully connected, tetrahedral arrangement of the dominant X-ray scatterers. FOCUS uses the estimated Fourier magnitudes obtained either by equipartitioning or by the FIPS method to calculate electron density maps determined from random starting phases. A peak search algorithm then assigns electron density to the tetrahedral atoms, which ordinarily are the most predominant electron-dense scatterers in zeotype materials. FOCUS produces a histogram of zeolite topologies in which the most frequently occurring structure is often the correct solution.

Here we report the synthesis boundaries, characterization, and structure solution by the FOCUS method of SSZ-58.

2. Experimental Section

2.1. Zeolite Synthesis. SSZ-58 was synthesized using the 1-butyl-1-cyclooctylpyrrolidinium cation (Figure 1) as a structure-directing agent (SDA). Generally, SSZ-58 was synthesized¹⁶ according to the method described in the example below by heating a mixture of the SDA, a silica source, sodium hydroxide, sodium borate decahydrate, and water. The molar composition of a representative synthesis gel is 0.05 Na₂O:0.10 (SDA)₂O:0.021 B₂O₃:41 H₂O:SiO₂.

In a typical synthesis, 6.9 g of 0.44 M aqueous solution of 1-butyl-1-cyclooctylpyrrolidinium hydroxide, 1.2 g of 1 N aqueous solution of sodium hydroxide, an additional 4 g of deionized water, and 0.06 g of sodium borate decahydrate were mixed in a 23-mL Teflon liner. The mixture was hand-stirred until the sodium borate was completely dissolved. Then, 0.9 g of CAB-O-SIL M-5 (98% SiO₂, 2% H₂O) was added to the mixture. After the mixture was thoroughly stirred, the Teflon liner was capped off, placed in a stainless steel Parr autoclave, and then heated in an oven at 160 °C while tumbling at about 43 rpm. The reaction was monitored periodically by measuring the pH of the reaction. Crystal formation was also monitored using scanning electron microscopy (SEM). The crystallization was typically completed after heating for 9 days. The collected solids were washed several times

with water and then rinsed with a minimal amount of acetone (10 mL) to remove any organic residues. The solids were allowed to air-dry overnight at room temperature and then dried in an oven at 120 °C for 1 h. The reaction yielded 0.8 g of SSZ-58. The SDA was then removed by a slow, staged calcination to 595 °C in an atmosphere of nitrogen containing 2% oxygen.

2.2. Analytical Methods. Preliminary powder X-ray diffraction (XRD) patterns were recorded on a Siemens D-500 instrument. Scanning electron micrographs (SEM) were recorded on a Hitachi S-570 instrument. Transmission electron micrographs (TEM) and electron diffraction patterns were obtained with a JEOL 2010 instrument operating at an accelerating voltage of 200 kV. Samples were prepared by dispersing the crystallites on a continuous carbon film.

Samples for detailed structural analysis were examined at Beamline X7A at Brookhaven National Laboratory. Data were collected at ambient temperature from 3 to 65° 2θ with a step size of 0.005° 2θ using a wavelength of 1.19941 Å. The X7A samples were prepared in 1.5-mm outer diameter glass capillaries that were sealed after being evacuated and heated overnight at 350 °C. The starting model for the Rietveld structure refinement was generated with the FOCUS algorithm. Initial distance least-squares refinements of the framework extracted from the FOCUS method were carried out with DLS-76.¹⁷ Energy minimizations of the SDA within the SSZ-58 framework were performed with Cerius² 2.1¹⁸ from MSI using the Burchart-Universal force field.¹⁹

Elemental analyses were performed by Galbraith Laboratories (Knoxville, TN). Thermogravimetric analysis (TGA) of the as-made B-SSZ-58 materials was performed on a Hi-Res TGA 2950 Thermogravimetric Analyzer (from TA Instruments). The sample was heated in air at a rate of 5 °C/min for the data collection.

¹³C NMR experiments were performed on a Bruker MSL 500 spectrometer using a 4-mm double resonance Bruker MAS probe. The samples were spun at the magic angle at 4.6 kHz. Spectra were collected with cross polarization from protons using a 90° pulse length of 5.25 μs. The spectra were insensitive to variations in contact time between 1 and 4 ms. A relaxation delay of 2 s was found to be sufficient for complete relaxation in the cases of both the pristine SDA and the SDA occluded within the zeolite. Typically 5000–8000 scans were acquired. The spectra were referenced to tetramethylsilane at 0 ppm. The data were processed with 50 Hz Lorentzian line broadening and zero-filled from 4096 to 8192 points. The tentative assignments of the SDA spectrum are based on literature chemical shifts from molecules with similar chemical groups.

The pore size and void volume of the calcined SSZ-58 were probed by physisorption of argon, nitrogen, and a series of hydrocarbon adsorbates. Argon adsorption at −186 °C was performed using the Micromeritics ASAP 2010. The sample was first outgassed at 400 °C for 16 h prior to argon adsorption. The low-pressure dose was 2.0 mL/g STP. A maximum of 1-h equilibration time per dose was used, and the total run time was 35 h. The free space of the sample tube was measured after the completion of the isotherm. This was done to prevent the trapping of helium in small pore zeolites, which can lead to significant errors in the measurement of the isotherm.²⁰ Deduction of pore dimensions from the adsorption isotherm was performed using density functional theory (DFT) as developed by Olivier^{21,22} for graphite slits, by the Saito–Foley adaptation of the Horvath–Kawazoe thermodynamic formulation,²³ and by the conventional *t*-plot method.²⁴ The *t*-plot

(12) Examples of these relationships include (a) the MTT and TON topologies: Thomas, J. M.; Millward, R.; White, D.; Subramanian, R. *J. Chem. Soc., Chem. Commun.* **1988**, 434 and (b) the MEL and MFI topologies: Thomas, J. M.; Millward, G. R. *J. Chem. Soc., Chem. Commun.* **1982**, 1380.
 (13) Grosse-Kunstleve, R. W.; McCusker, L. B.; Baerlocher, C. *J. Appl. Crystallogr.* **1997**, *30*, 985.
 (14) Grosse-Kunstleve, R. W. Dissertation ETH No. 11422, 1996.
 (15) Falcioni, M.; Deem, M. W. *J. Chem. Phys.* **1999**, *110*, 1754.
 (16) Elomari, S. PCT U.S. Patent 02/21172.

(17) Baerlocher, C.; Hepp, A.; Meier, W. M. *DLS-76*; ETH: Zurich, Switzerland, 1977.
 (18) Cerius² 2.1. Product of MSI and Biosym.
 (19) (a) Rappe, A. K.; Casewit, C. J.; Colwell, K. S.; Goddard, W. A., III; Skill, W. M. *J. Am. Chem. Soc.* **1992**, *114*, 10024. (b) de Vos Burchart, E. Studies on Zeolites: Molecular Mechanics, Framework Stability and Crystal Growth, Table 1, Chapter XII. Ph.D. Thesis, 1992.
 (20) Groen, J. C.; Peffer, L. A. A. Influence of Dead Space Measurement on Adsorption Characteristics of Microporous Zeolites. *Micro Rep.* **1997**, *8*, 8.
 (21) Olivier, J. P. *J. Porous Mater.* **1995**, *2*, 9.
 (22) Olivier, J. P. *Carbon* **1998**, *36*, 1469.
 (23) Saito, A.; Foley, H. C. *Microporous Mater.* **1995**, *3*, 531.

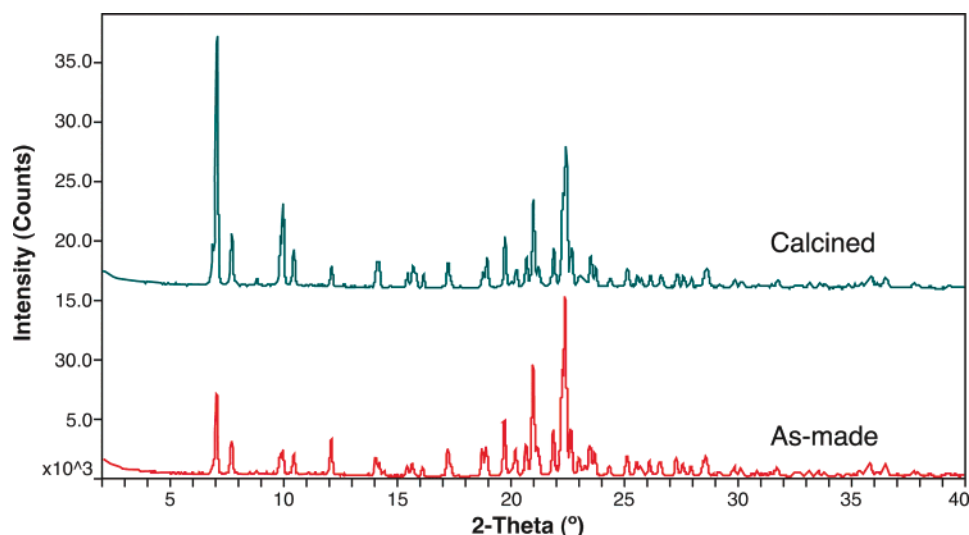


Figure 2. Powder X-ray diffraction patterns of as-made (bottom) and calcined (top) SSZ-58.

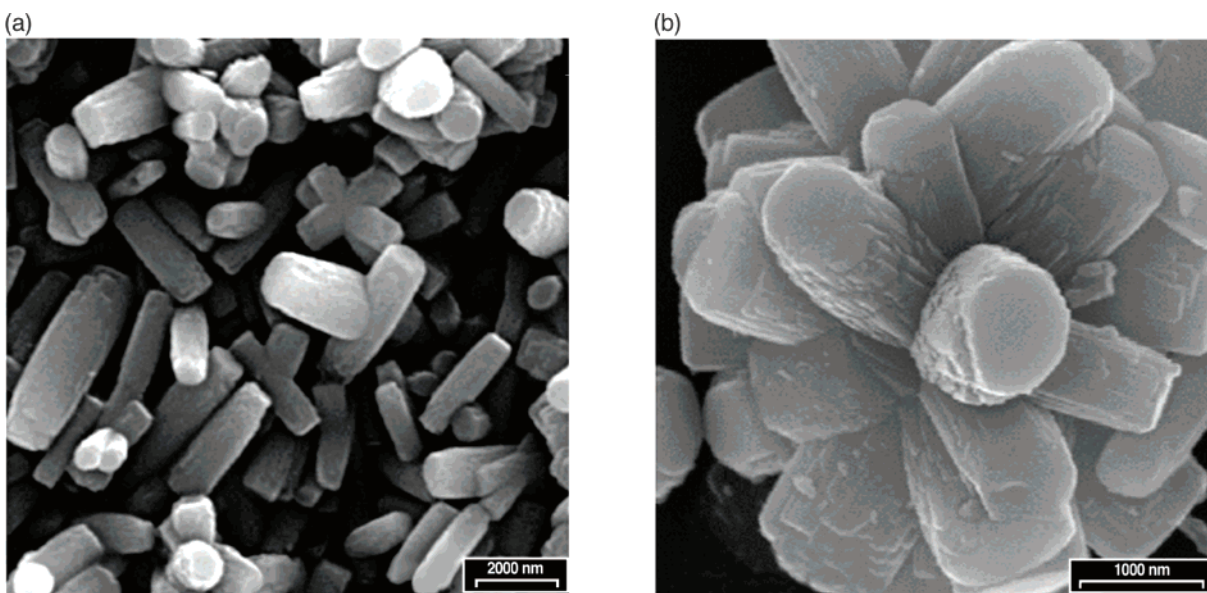


Figure 3. Scanning electron micrographs of SSZ-58.

analysis was also performed using nitrogen adsorption data collected by the Micromeritics 2400 instrument.

The adsorption capacities of zeolites for vapor-phase hydrocarbons were measured at room temperature using a Cahn C-2000 balance. *n*-Hexane, cyclohexane, 2,2-dimethylbutane, and 1,3,5-triisopropylbenzene were used as “plug gauge” adsorbate molecules with various kinetic diameters. Detailed discussion on hydrocarbon adsorption experiments is reported elsewhere.²⁵

3. Results and Discussion

3.1. Characterization by Powder X-ray Diffraction, Electron Diffraction, and Electron Microscopy. Figure 2 shows the powder XRD (Cu K α) patterns of the as-made and calcined forms of the novel zeolite SSZ-58. The diffraction patterns indicate SSZ-58 remains crystalline after calcination. SEM micrographs (Figure 3) show that the basic morphology of the

crystals is in the form of rods approximately 2.5 μm long and 0.5 μm wide. While there are many individual rods (Figure 3a), intergrown crystals are also common (Figure 3b).

Diffraction peaks from the synchrotron data (Figure 4) were fitted using the pseudo-Voigt function of Thompson et al.²⁶ with the asymmetry correction developed by Finger et al.²⁷ The fitted 2θ peak positions were used as input to the powder diffraction pattern indexing programs ITO,²⁸ TREOR99,²⁹ and DICVOL.³⁰ Each program produced the same orthorhombic unit cell: $a = 25.112 \text{ \AA}$, $b = 12.498 \text{ \AA}$, $c = 12.860 \text{ \AA}$. The figures of merit (FOM) of the selected unit cell in the DICVOL program were $M_{20} = 105$ ³¹ and $F_{20} = 341$.³² These high agreement values indicate a likely unit cell. The XRD patterns of both the as-

(26) Thompson, P.; Cox, D. E.; Hastings, J. B. *J. Appl. Crystallogr.* **1987**, *20*, 79.

(27) Finger, L. W.; Cox, D. E.; Jephcoat, A. P. *J. Appl. Crystallogr.* **1994**, *27*, 892.

(28) Visser, J. W. *J. Appl. Crystallogr.* **1969**, *2*, 89.

(29) Werner, P. E.; Eriksson, L.; Westdahl, M. *J. Appl. Crystallogr.* **1985**, *18*, 367.

(30) Boulton, A.; Louer, D. *J. Appl. Crystallogr.* **1991**, *24*, 987.

(31) de Wolff, P. M. *J. Appl. Crystallogr.* **1968**, *1*, 108.

(32) Smith, G. L.; Snyder, R. L. *J. Appl. Crystallogr.* **1979**, *12*, 60.

(24) Lippens, B. C.; Boer, J. H. D. *J. Catal.* **1965**, *4*, 319.
 (25) Chen, C. Y.; Zones, S. I. Zeolites and Mesoporous Materials at the Dawn of the 21st Century. Proceedings of the 13th International Zeolite Conference, Montpellier, France, 8–13, July, 2001; In *Studies in Surface Science and Catalysis*; Galarneau, A., Di Renzo, F., Fajula, R., Vedin, J., Eds.; Elsevier: Dordrecht, The Netherlands, 2001; Vol. 135, p 222.

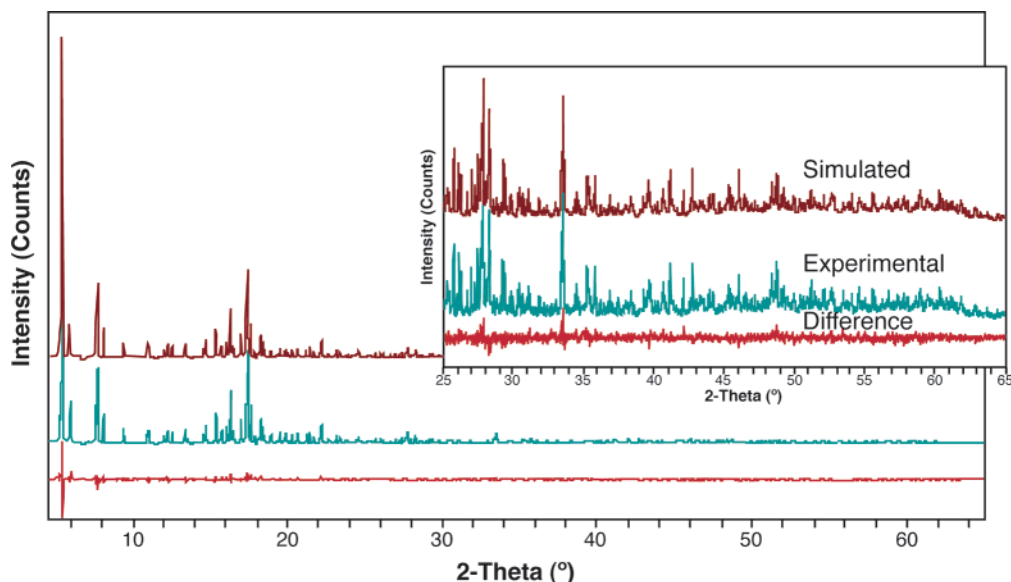


Figure 4. Simulated (top), experimental (middle), and difference (bottom) profiles for the synchrotron X-ray ($\lambda = 1.19941 \text{ \AA}$) powder diffraction pattern of calcined SSZ-58. Note that the regions from 6.7 to 7.0, 11.4 to 11.7, 13.7 to 13.95, and 17.90 to 18.07° 2θ were excluded due to the slight presence of SSZ-57.

Table 1. Observed and Calculated Positions of First 20 Observed Reflections in the Powder XRD Pattern of Calcined SSZ-58

<i>hkl</i>	2θ (observed, $\lambda = 1.19941 \text{ \AA}$)	2θ (calculated, $\lambda = 1.19941 \text{ \AA}$)	2θ (calculated, $\lambda = 1.5418 \text{ \AA}$)
001	5.348	5.349	6.878
200	5.478	5.478	7.044
101	6.014	6.010	7.728
201	7.659	7.659	9.850
210	7.768	7.767	9.989
111	8.153	8.152	10.485
211	9.436	9.435	12.137
400	10.969	10.968	14.113
102	11.057	11.055	14.225
012	12.044	12.047	15.505
401	12.213	12.210	15.715
220	12.317	12.312	15.847
121	12.562	12.559	16.165
411	13.403	13.401	17.252
221	13.435	13.432	17.292
312	14.602	14.602	18.804
501	15.741	15.741	20.277
003	16.092	16.093	20.732
103	16.328	16.327	21.035

made and calcined forms can be indexed in a similar orthorhombic unit cell, suggesting there are no symmetry changes after removal of the SDA. Table 1 shows the observed and calculated positions of the first 20 observed *hkl* reflections. The systematic absences (*hk0*, $h = 2n$) narrow the likely space groups to *Pmma*, *Pm2a*, or *P2₁ma*. Since *a* is nearly twice *b*, it was not completely certain from the powder XRD patterns whether *0k0* reflections with odd values of *k* are allowed. However, the electron diffraction data indicate the *0l0* reflection is present, thereby ruling out systematic absences among the *0k0* reflections and allowing consideration to be limited to the abovementioned space groups. We focused our attention on *Pmma* because the lower symmetry of the other possible space groups would require an inordinately large number of tetrahedral (T) atoms in the asymmetric unit.

Electron diffraction and imaging data obtained using TEM support the proposed unit cell. Figure 5a shows the [010] zone axis pattern. It exhibits a set of orthogonal diffraction spots with the largest *d* spacings of 25 and 12.9 Å. The corresponding

lattice fringe image is shown in Figure 5b. Figure 5c is an electron diffraction pattern showing another set of orthogonal diffraction spots whose *d* spacings are 12.5 and 12.9 Å. This corresponds to the view along the [100] zone axis. Figure 5d is the corresponding low magnification TEM image. In the JEOL 2010, there is no relative rotation between the electron diffraction pattern and the image. This image therefore indicates that the length of the crystal is parallel to the 12.5 Å lattice fringes and the end faces are parallel to the 12.9 Å fringes. Another HREM image of the same orientation is shown in Figure 5e. Figure 5f shows a strong set of 12.9 Å lattice fringes that were verified to be parallel to the end crystal face.

3.2. Structure Solution with FOCUS. The framework topology of SSZ-58 was determined with the FOCUS Fourier recycling method. Peak intensities were extracted from the powder pattern using the LeBail method in GSAS.³³ The lattice parameters, space group, and peak magnitudes were then used as input to FOCUS. Peaks between 5 and 60° 2θ (resolution of 1.2 Å) were included in the structure solution. Figure 6 shows projections along each cell axis of the predominant framework structure (without oxygen atoms) obtained from the FOCUS topology search. The DLS *R*-value of this framework was 0.4%, indicating a chemically sensible structure. This topology has 12 T atoms and 26 O atoms per asymmetric unit, 18.3 T atoms/1000 Å³, and a calculated density of 1.83 g/cm³. In terms of the number of T atoms in the asymmetric unit of its topological symmetry, SSZ-58 is the most complex zeolite or zeotype structure solved from powder diffraction data. ZSM-5 (MFI),³⁴ which has 12 T atoms in its asymmetric unit, was solved from single-crystal data using model building. Only SSZ-23 (STT), whose structure was determined from single-crystal data, possesses a more complex zeolite framework with 16 T atoms in its asymmetric unit.⁵

3.3. Rietveld Refinement. Because of the slight presence of SSZ-57³⁵ zeolite in our sample, the regions from 6.7 to 7.0,

(33) Larson, A. C.; von Dreele, R. B. *General Structure Analysis System GSAS*; Los Alamos National Laboratory: Los Alamos, NM, 1994.

(34) Olson, D. H.; Kokotailo, G. T.; Lawton, S. L.; Meier, W. M. *J. Phys. Chem.* **1981**, *85*, 2238.

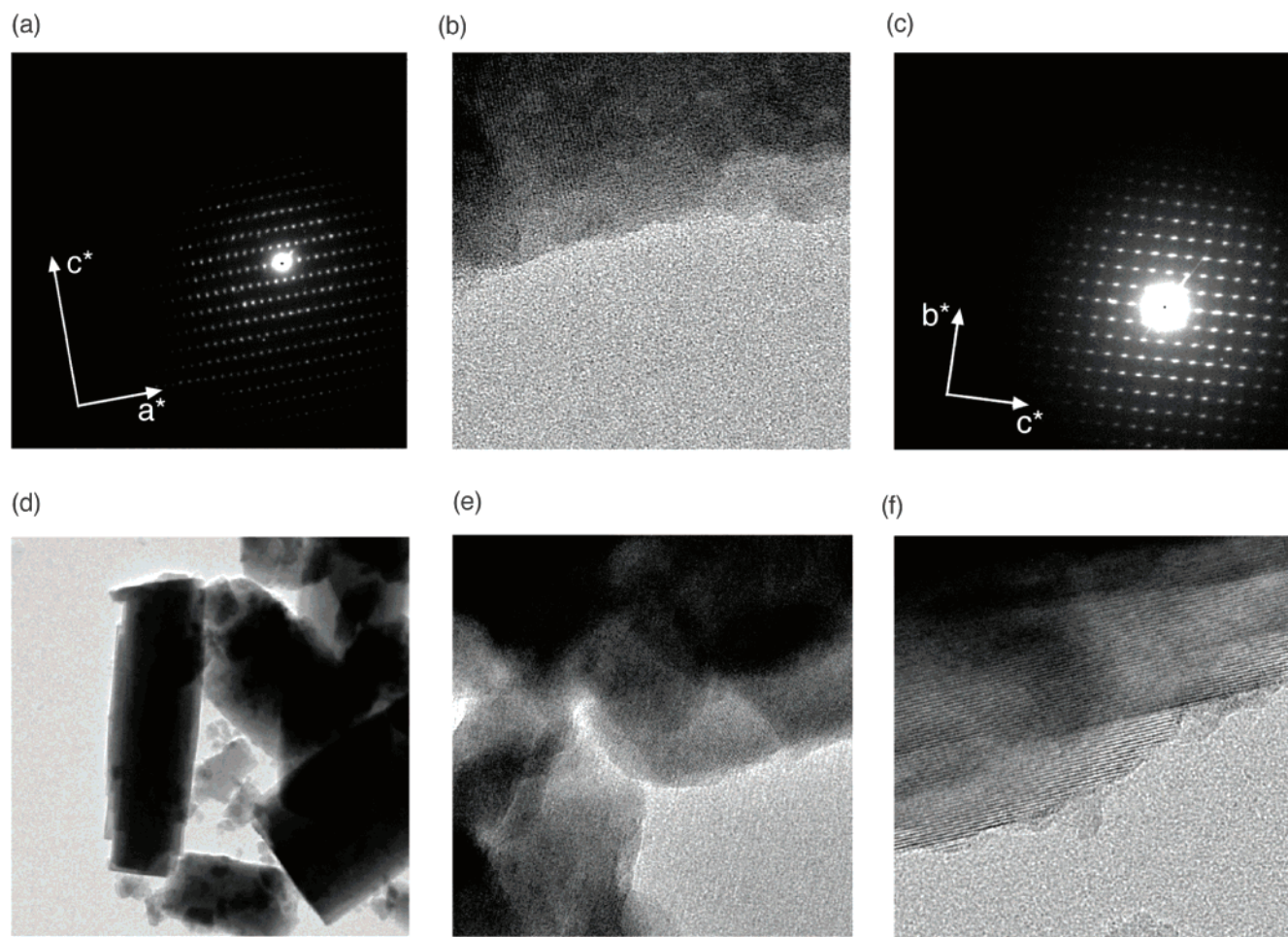


Figure 5. (a) Electron diffraction pattern of SSZ-58 along the [010] zone axis. (b) Corresponding lattice fringe image along the [010] zone axis. (c) Electron diffraction pattern of SSZ-58 along the [100] zone axis. (d) The corresponding low magnification TEM image along the [100] zone axis. (e) A high-resolution electron microscope image of the same orientation in (d). (f) Corresponding lattice fringe image showing the 12.9 Å fringes.

11.4 to 11.7, 13.7 to 13.95, and 17.90 to 18.07° 2θ (see Figure 4) were excluded from the Rietveld refinement. Although data were available for pure preparations of SSZ-58, this sample was chosen for refinement because it possessed superior crystallinity and there was minimal overlap with the most intense peaks of the novel SSZ-57 phase. The initial atomic positions for the starting model were determined by a DLS refinement of the unit cell obtained from FOCUS. A 12-term Chebyshev function was used to model the background. Atoms of identical element type were constrained to have the same isotropic thermal displacement parameters. Soft distance restraints ($\text{Si}-\text{O} = 1.60 \pm 0.03 \text{ \AA}$, $\text{O}-\text{O} = 2.61 \pm 0.03 \text{ \AA}$) were placed on the bonds between the silicon and oxygen atoms and the distances between the tetrahedral oxygen atoms.

At the completion of the refinement, no electron density above 0.5 e/\AA^3 could be observed around any framework atoms in the difference Fourier maps. Supporting Information Table 1S summarizes the final details of the refinement, and Table 2 shows the atomic parameters obtained from the refinement. Figure 4 shows excellent agreement between the simulated pattern and the experimental data. The final agreement values for the refinement are $R_p = 7.25\%$ and $R_{wp} = 8.42\%$.

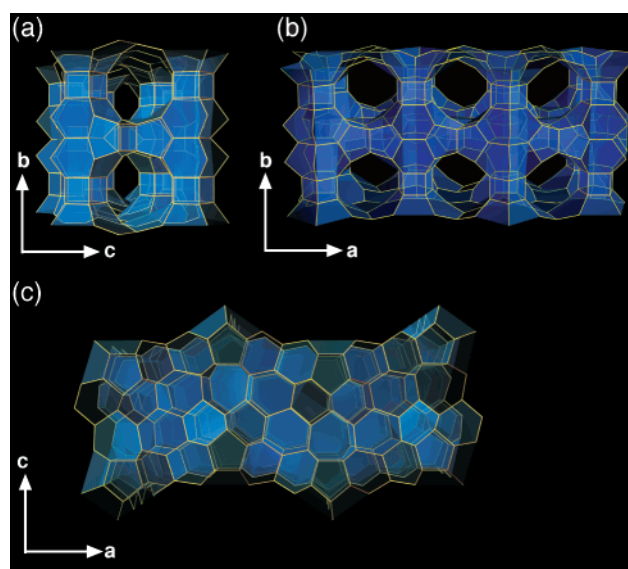


Figure 6. Projections of the SSZ-58 unit cell along (a) the a -axis, (b) the c -axis, and (c) the b -axis. Oxygen atoms are removed for clarity. Figures were created as 3D models by Kelly and Scott Harvey with proprietary software, FormZ, and Electric Image.

Details on the atomic distances and angles can be found in Supporting Information Tables 2S and 3S. The average Si–O bond distance is 1.58 Å with a minimum of 1.55 Å and a

(35) Elomari, S. United States Patent Application, Publication No. U.S. 2002/0081262 A1, 2002.

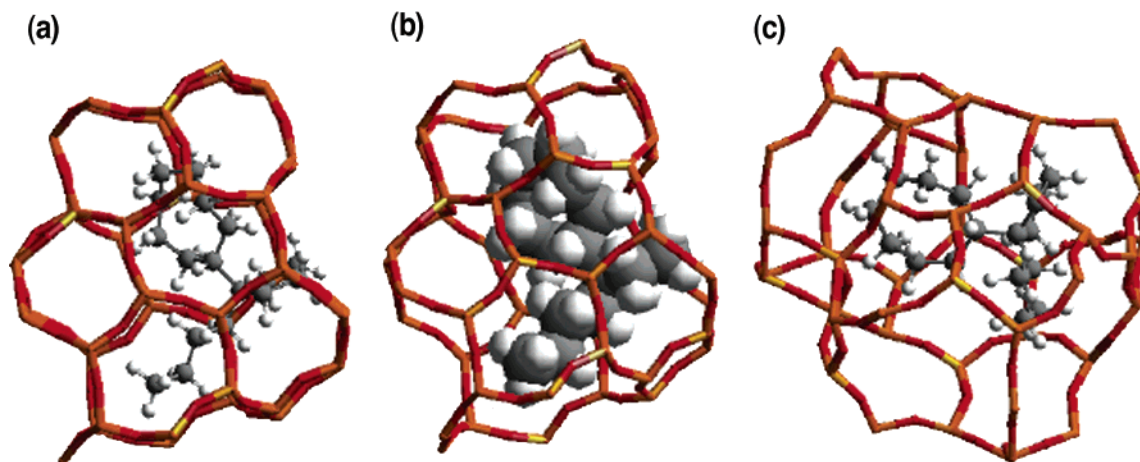


Figure 7. Energy-minimized configuration of the 1-butyl-1-cyclooctylpyrrolidinium SDA within the cavity at the channel intersections of SSZ-58. (a) Ball-and-stick model of SDA to emphasize the atom positions, (b) spherical model of SDA to emphasize the space-filling of the SDA within the cavity, and (c) same view as (a) except with cage tilted slightly upward to offer another view. Figures were generated with Cerius2 software from Biosym and MSI.

Table 2. Refined Atomic Parameters of SSZ-58 in Space Group *Pmma*; $a = 25.1106 \text{ \AA}$, $b = 12.4972 \text{ \AA}$, $c = 12.8596 \text{ \AA}$

atom	<i>x</i>	<i>y</i>	<i>z</i>	U_{iso} (\AA^2)	multiplicity	atom	<i>x</i>	<i>y</i>	<i>z</i>	U_{iso} (\AA^2)	multiplicity
Si1	0.135(2)	0.1903(5)	0.3452(4)	0.0238	8	O8	0.0744(5)	0.192(1)	0.8642(7)	0.0377	8
Si2	0.1527(2)	0.1228(3)	0.1152(4)	0.0238	8	O9	0.0218(4)	0.176(1)	0.6937(9)	0.0377	8
Si3	0.0788(2)	0.1939(6)	0.7417(5)	0.0238	8	O10	0.1183(3)	0.1054(3)	0.705(1)	0.0377	8
Si4	0.1528(3)	0.3759(5)	0.6827(5)	0.0238	8	O11	0.1011(4)	0.3115(8)	0.711(1)	0.0377	8
Si5	0.1898(3)	0	0.4540(6)	0.0238	4	O12	0.1370(7)	1/2	0.683(2)	0.0377	4
Si6	0.1523(3)	0	0.6846(6)	0.0238	4	O13	0.1762(5)	0.346(1)	0.5720(8)	0.0377	8
Si7	0.0196(3)	0.1246(3)	0.3846(4)	0.0238	8	O14	0.1970(4)	0.347(1)	0.7653(9)	0.0377	8
Si8	0.1887(3)	0.3771(5)	0.4553(5)	0.0238	8	O15	0.1807(5)	0	0.5731(6)	0.0377	4
Si9	1/4	0.2030(6)	0.9885(5)	0.0238	4	O16	1/4	0	0.422(2)	0.0377	2
Si10	1/4	0	0.8404(6)	0.0238	2	O17	0.1979(2)	0	0.7712(6)	0.0377	4
Si11	0.0572(2)	0.1262(5)	0.9628(5)	0.0238	8	O18	0	0.144(1)	1/2	0.0377	4
Si12	1/4	0.3749(7)	0.8274(8)	0.0238	4	O19	0.0203(7)	0	0.361(1)	0.0377	4
O1	0.1624(4)	0.1056(3)	0.4149(9)	0.0377	8	O20	1/4	0.349(2)	0.437(2)	0.0377	4
O2	0.0735(3)	0.185(1)	0.374(1)	0.0377	8	O21	0.1785(7)	1/2	0.429(2)	0.0377	4
O3	0.1538(5)	0.3097(9)	0.3766(9)	0.0377	8	O22	1/4	0.316(1)	0.937(2)	0.0377	4
O4	0.1477(5)	0.175(1)	0.2274(5)	0.0377	8	O23	1/4	0.1039(3)	0.9114(7)	0.0377	4
O5	0.1988(1)	0.1854(9)	0.0559(7)	0.0377	8	O24	0	0.162(1)	0	0.0377	4
O6	0.1679(5)	0	0.1197(1)	0.0377	4	O25	0.0594(8)	0	0.927(2)	0.0377	4
O7	0.0987(4)	0.1429(9)	0.0535(9)	0.0377	8	O26	1/4	1/2	0.857(2)	0.0377	2

maximum of 1.64 \AA . While the distance of 1.56 \AA (observed for Si5) is below the optimal Si–O distance of 1.61 \AA , it is not unusual in reports of zeolite structures. We considered the possibility that boron may preferentially substitute at this site, but attempts to refine partial occupancies of boron and silicon in this position did not improve the refinement. We are currently investigating aluminosilicate samples of SSZ-58 to examine how the presence of aluminum affects the bond distances around different T sites.

The minimum and maximum O–Si–O tetrahedral angles are 103.6° and 116.6° respectively, and the average tetrahedral angles are all within 0.1° of 109.5° . The average $\langle \text{Si–O–Si} \rangle$ angle is 155° with a minimum and maximum of 144° and 176° . The 176° angle is associated with atoms (Si10 and O23) positioned on high-symmetry positions. This may imply that either there is disorder associated with these atoms or the actual symmetry of the model is lower than the *Pmma* space group. Reducing the symmetry of the model could improve the wide Si–O–Si bond angle. However, we feel that doubling the number of atomic parameters would make the powder data unacceptably underdetermined in a system for which there is already excellent agreement with the presented model. Nonetheless, the numerical and graphical agreement between the model and experimental data leave no doubt that the important structural details of the topological model are correct.

3.4. Structure of SSZ-58. SSZ-58 possesses a two-dimensional system of pores (Figure 6) that intersect to form large cavities (Figure 7) that are bound by two pairs of opposing 10-membered rings. The pores along the *c*-direction (Figure 6b) are straight channels bound by 10-membered rings with dimensions of $5.7 \times 5.2 \text{ \AA}$ assuming an oxygen radius of 1.35 \AA . The sinusoidal pores along the *a* direction (Figure 6a) are bound by distorted elliptical 10-membered rings with dimensions of $4.8 \times 5.7 \text{ \AA}$. The central cavity is circumscribed by a 12- and a 16-membered ring with dimensions of about $8.0 \text{ \AA} \times 5.9 \text{ \AA}$ and $11.6 \text{ \AA} \times 6.4 \text{ \AA}$, respectively. The approximately planar 12- and 16-membered rings are nearly perpendicular to each other.

There are some noteworthy similarities between the structures of SSZ-58 and MCM-22 (MWW).³⁶ While the MWW framework has two nonintersecting 10-membered ring channel systems and SSZ-58 has a single-channel system, these are the only zeolites to possess two-dimensional channel systems of 10-membered ring pores. Both structures are composed of layers (Figure 6c shows a projection of such a layer in SSZ-58) connected by simple structural units. However, in MCM-22 the layers are linked by double 6-membered ring (D6R or 6^2_4) subunits, whereas in SSZ-58 the layers are joined by double

(36) Cambor, M. A.; Corma, A.; Diaz-Cabanas, M. J.; Baerlocher, C. *J. Phys. Chem. B* **1998**, *102*, 44.

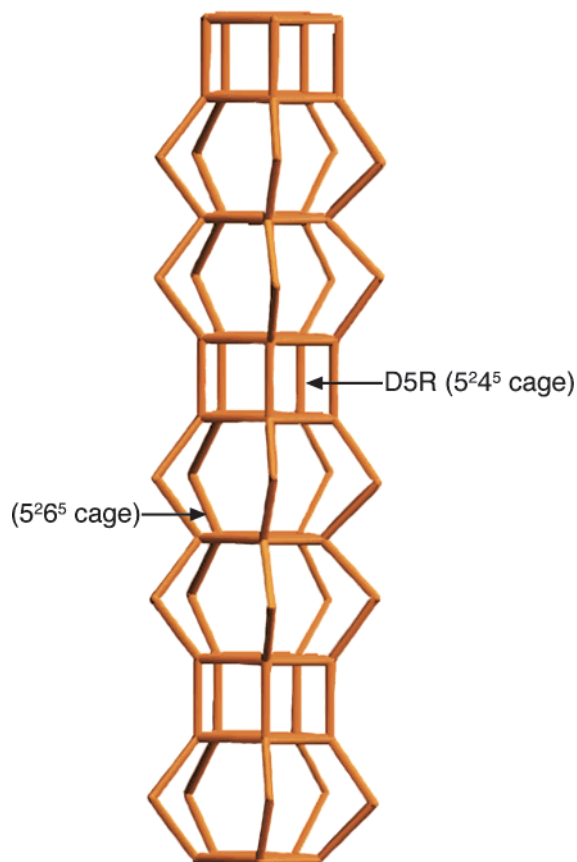


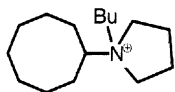
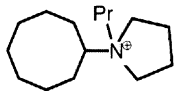
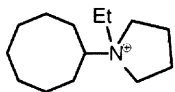
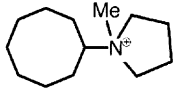
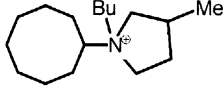
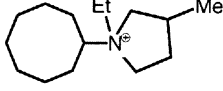
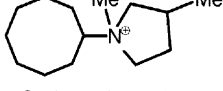
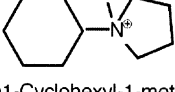
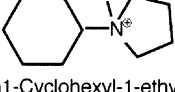
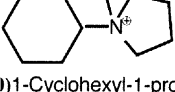
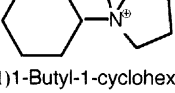
Figure 8. View of the columnar units that link to form the framework of SSZ-58. Note the $5^2 6^5$ and $5^2 4^5$ cages from which the columns are built. Figures were generated with Cerius2 software from Biosym and MSI.

5-membered ring (D5R or $5^2 4^5$) subunits (this description is not a reflection of possible growth mechanisms in either zeolite).

Although the D5R is a simple building unit, it surprisingly has not been observed in any other zeolite structures. However, Groenen and co-workers³⁷ have detected D5R silicate anions by ^{29}Si NMR in tetraalkylammonium hydroxide/silicate solutions. In fact, they were able to isolate the silicate species by trimethylsilylation of the silicate anions and subsequently detect the trimethylsilylated products using gas chromatography and mass spectrometry. Although D5R subunits are not present in the frameworks of ZSM-5 and ZSM-11, Groenen et al. speculated that ZSM-5 and ZSM-11 may form by condensation of these D5R subunits. Another previously unseen feature in SSZ-58 is the $5^2 6^5$ cage (Figure 8). The $5^2 6^5$ and $5^2 4^5$ cages stack along the *b*-direction to form columns (Figure 8) that are connected to neighboring columns primarily by four-membered ring units.

3.5. The As-Made Zeolite. Elemental analyses of the as-made borosilicate SSZ-58 indicated a Si/B ratio of 32 with wt % of 8.18, 0.61, and 1.42 for C, N, and H, respectively, which corresponds to a molar ratio of 15.6 C:1 N:32.6 H. Note that this molar ratio compares favorably with the molar ratio expected from the chemical formula of the SDA: $\text{C}_{16}\text{NH}_{32}$. On the basis of carbon content, the Si/SDA ratio is 35, which is nearly equivalent to the Si/B ratio of the product. This corresponds to approximately 2 SDA molecules per unit cell (vide supra) of SSZ-58. Although other SSZ-58 samples were pre-

Table 3. Structure-Directing Agents (SDAs) Related to the 1-Butyl-1-cyclooctylpyrrolidinium Cation and the Products of Their Zeolite Syntheses

SDA	Zeolitic Product
	SSZ-58
	Impure phase of SSZ-58
	ZSM-12 (MTW)
	ZSM-12 (MTW)
	ZSM-11 (MEL)
	ZSM-11 (MEL)
	EU-1 (EUO)
	ZSM-12 (MTW)
	ZSM-12 (MTW)
	Impure phase of an unknown (SSZ-57)
	Unknown (SSZ-57)

(37) Groenen, E. J. J.; Kortbeek, A. G. T. G.; Mackay M.; Sudmeijer, O. *Zeolites* **1986**, *6*, 403.

pared with lower boron contents, the chemical analyses strongly suggest, in this particular sample, that most of the charge on

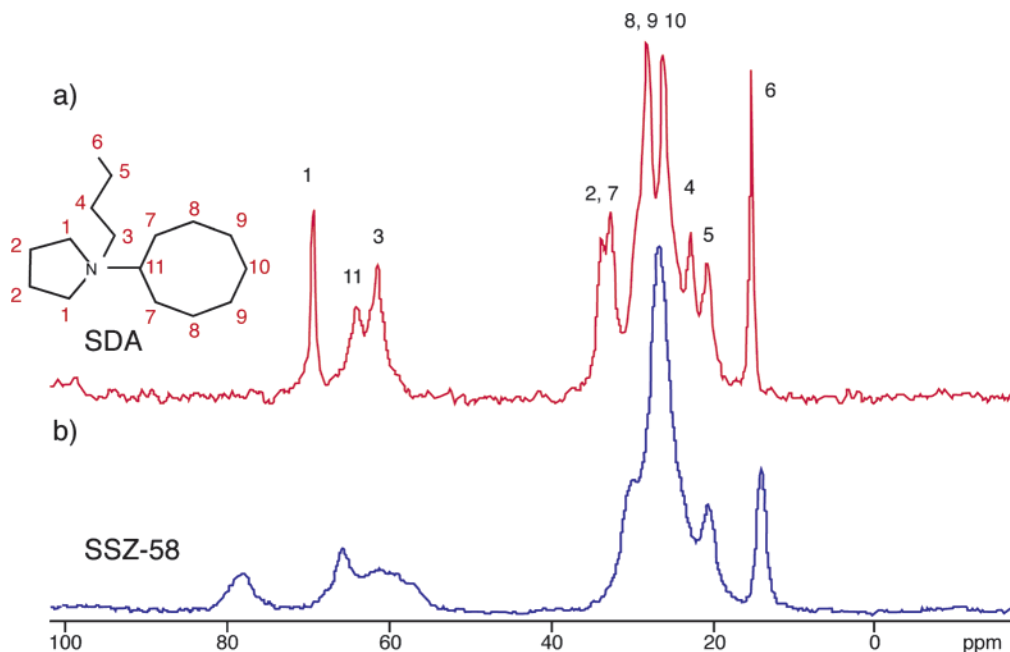


Figure 9. Solid-state ^{13}C NMR spectra of (a) the solid SDA in its salt form and (b) of the SDA included within zeolite SSZ-58.

the SDA is compensated by the framework boron in the as-made material. In the TGA experiment there is a 10.5% mass loss event between 270 and 600 °C that corresponds to the combustion of the organic SDA. This mass loss is in excellent agreement with the organic content determined from chemical analysis.

The ^{13}C CP MAS NMR spectrum from the SDA molecule and its tentative assignments are shown in Figure 9a. The intensities of the peaks are not quantitative as they are affected by cross polarization dynamics. However, it appears that all the carbon atoms can be observed using this experiment. Figure 9b shows the ^{13}C CP MAS spectrum from the organic occluded in the zeolite framework. Peak broadening clearly occurs once the SDA is trapped in the inorganic framework, but the integrity of the organic appears to be maintained after occlusion within the zeolite. Broadening can arise from decreased mobility of the SDA molecule within the framework due to steric restrictions.

3.6. SDA Selectivity. The chemical analyses, TGA measurement, and ^{13}C NMR experiments indicate that there is an occluded SDA molecule for each cavity in the zeolite structure. This suggests a high specificity between the 1-butyl-1-cyclooctylpyrrolidinium cation and the SSZ-58 framework. The 1-butyl-1-cyclooctylpyrrolidinium cation is very selective for the crystallization of SSZ-58. However, the slightest modification to the structure of the SDA profoundly affects the product of the zeolite synthesis. Table 3 shows some related SDAs that were investigated along with their zeolitic products. In general, it is observed that decreases in the size of the *n*-alkyl chain (either methyl or ethyl) and decreases in the size of the cycloalkyl substituent result in **MTW**. Attachment of a methyl group to the 3-position of the pyrrolidine ring yields either **MEL** or **EUO** phases (Figure 10). Replacement of the cyclo-octyl ring with a cyclo-hexyl ring yields the novel zeolite SSZ-57.

Given the specificity of the 1-butyl-1-cyclooctylpyrrolidinium cation for crystallizing SSZ-58, we thought it would be interesting to compare the stabilization energies of the SDA

Table 4. Stabilization Energies Calculated for the 1-Butyl-1-cyclooctylpyrrolidinium Cation within the Frameworks of SSZ-58 and Other Zeolites Synthesized with Similar Structure-Directing Agents

framework	number of SDA molecules/unit cell	stabilization energy (kJ/mol SDA)	stabilization energy (kJ/mol T Atoms)
SSZ-58	2	-181	-4.9
ZSM-11	2	-145	-3.0
EU-1	2	-159	-2.8
ZSM-12	1	-2	-0.03

molecule within the framework of SSZ-58 with other zeolites synthesized when the identity of either the alkyl chain or the cyclic group are varied. Energy minimizations were performed to determine the optimal configuration of the SDA within the structures of SSZ-58, ZSM-12, ZSM-11, and EU-1. Stabilization energies were determined by calculating the difference in energies of the free molecule and the molecule occluded within the zeolite framework. The positions of framework atoms were fixed during the energy minimizations. Contributions from (1) van der Waals interactions and (2) valence bond, angle, and torsion energies were determined with the Burchart-Universal force field. Coulombic interactions between the cation and the zeolite framework were neglected.

At least 10 different configurations of the SDA were sampled for each framework by placing the molecule in random locations within the void space of the zeolite. In the case of SSZ-58, over 30 configurations were examined. Since the other frameworks offer a limited number of possible configurations for the molecule, their optimal positions were found quite readily. The energy we report for each framework (Table 4) is the minimum found among the configurations sampled. In SSZ-58 and ZSM-11, two SDA molecules were placed in each unit cell (two molecules per cavity or channel intersection). EU-1 possesses a one-dimensional 10-membered ring pore with side pockets. Four molecules per unit cell were initially chosen for EU-1 since there are four side pockets per unit cell. However, the energy calculations indicated there is insufficient space to allow neighboring side pockets to be occupied by the 1-butyl-1-

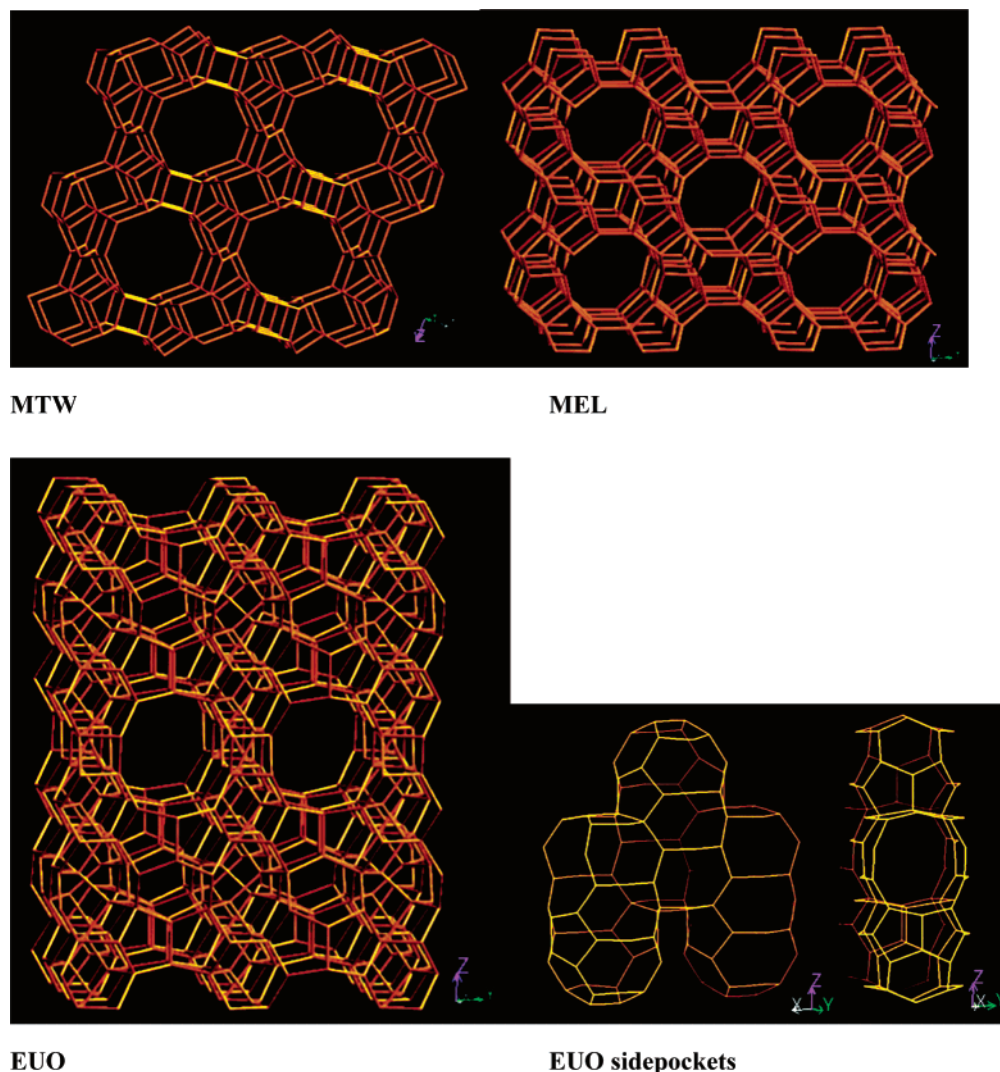


Figure 10. Framework topologies of MTW, MEL, and EUO. Figures are from International Zeolite Association website (<http://www.iza-structure.org>) and are used with permission of IZA.

cyclooctylpyrrolidinium cation. Therefore, we again performed the energy minimizations for two SDA molecules/unit cell. The unit cell of ZSM-12 possesses a 5.0 Å repeat distance parallel to the pore direction. Since this distance is smaller than the dimensions of the SDA molecule, energy minimizations were performed using supercells created by stacking between two- and four-unit cells in the pore direction.

Table 4 shows SSZ-58 is the most energetically favorable host for the 1-butyl-1-cyclooctylpyrrolidinium cation. Compared with similar calculations of other zeolite guest/host systems,³⁸ the stabilization energy (−181 kJ/mol SDA, −4.9 kJ/mol Si) indicates a highly favorable interaction between the framework and the SDA. Figure 7 demonstrates the geometric complementarity between the energy-optimized SDA and the cavity positioned at the intersecting channels of SSZ-58. While the SDA is only slightly less stabilized in the frameworks of ZSM-11 and EU-1 than in SSZ-58, there is a significantly larger stabilization of the silica framework in the case of SSZ-58. These calculations are consistent with the high specificity of the

1-butyl-1-cyclooctylpyrrolidinium cation for the synthesis of SSZ-58.

3.7. Adsorption in SSZ-58. SSZ-58 has a micropore volume of 0.13 cm³/g as determined from argon adsorption by the conventional *t*-plot method. We also analyzed the adsorption data using Olivier's DFT model for graphite slits to deduce the pore dimensions of SSZ-58. Despite the differences in pore geometry, this model does give directional guidance when applied to zeolites, particularly when the "pore radius" is interpreted as representing the local radius of curvature. For straight cylindrical channels the local radius of curvature is indeed the pore radius.

The DFT model for SSZ-58 indicates that about 70% of the microporosity has a diameter of about 5.2 Å with the remaining porosity having a pore diameter of 7.2 Å. The proposed structure is consistent with these experimental deductions. The two 10-membered ring channels correspond to the microporosity having diameters of ca. 5.2 Å, and the curvatures of the cavities at the channel intersections correspond to the 7.2 Å peak in the DFT data.

SSZ-58 was also studied with vapor-phase hydrocarbon adsorption and compared with the following five groups of

(38) Examples include (a) Lobo, R. F.; Davis, M. E. *J. Am. Chem. Soc.* **1995**, *117*, 3766 and (b) Nery, J. G.; Hwang, S.; Davis, M. E. *Microporous Mesoporous Mater.* **2002**, *52*, 19.

Table 5. Adsorption Capacities for SSZ-58 and Other Zeolites Investigated in This Work: (I) *n*-Hexane, (II) Cyclohexane, (III) 2,2-Dimethylbutane, and (IV) 1,3,5-Triisopropylbenzene

adsorbate	kinetic diameter, Å	adsorption capacity, cm ³ /g					
		UTD-1	SSZ-33	SSZ-58	ZSM-5	SSZ-37	SSZ-32
I	4.4	0.121	0.202	0.132	0.172	0.159	0.075
II	5.0	0.111	0.198	0.133	0.152	0.153	0.011
III	6.2	0.119	0.197	0.118	0.147	0.064	0.012
IV	8.5	0.111	0.035	0.007	0.015	0.025	-

zeolites, which possess different dimensionalities of channel systems and different pore sizes and shapes: (1) 14-membered ring zeolite UTD-1 (similar to **DON**), (2) zeolite with an intersecting 12-/12-/10-membered ring channel system: SSZ-33 (similar to **CON**), (3) 10-membered ring zeolite with three-dimensional channels: ZSM-5 (**MFI**), (4) zeolite with medium-pore channels connected by 12-membered ring windows: SSZ-37 (**NES**), (5) 10-membered ring zeolite with one-dimensional channels: SSZ-32 (**MTT**).

The results from hydrocarbon adsorption experiments of these zeolites are shown in Table 5.

As shown in Table 5, the 14-membered ring zeolite UTD-1 readily adsorbs the bulky 1,3,5-triisopropylbenzene (135-TIPB). Also note that its 135-TIPB adsorption capacity is nearly equivalent to the cyclohexane and 2,2-dimethylbutane adsorption capacities. This demonstrates that most of the micropore volume in UTD-1 available to these smaller adsorbate molecules is also accessible by 135-TIPB. However, adsorption capacities for 135-TIPB are lower than for hexane, cyclohexane, and 2,2-dimethylbutane in the zeolite SSZ-33. These results indicate that the effective size and shape of the pore openings in these 14- or 12-membered ring zeolites become critical to the diffusion of 135-TIPB molecules. Apparently, this bulky molecule does not penetrate the 10-membered ring pore openings of zeolites such as ZSM-5, SSZ-37, or SSZ-32. These data are consistent with the low adsorption for 135-TIPB observed in the 10-membered ring pore system of SSZ-58.

In the same respect that adsorption of 135-TIPB may discriminate the dimensions of 12- and 14-membered ring pore zeolites, adsorption of 2,2-dimethylbutane proves useful for distinguishing 10-membered ring zeolites from larger-pore zeolites. In the cases of the 10-membered ring pore zeolites listed in Table 5, there is a decrease in measured adsorption capacity in going from cyclohexane or *n*-hexane to 2,2-dimethylbutane. On the basis of comparison of the adsorption results in SSZ-58 for 2,2-dimethylbutane, *n*-hexane, and cyclohexane with those of the other zeolites in Table 5, SSZ-58 appears to be a 10-membered ring zeolite possessing either a multidimensional pore system or a one-dimensional system with side pockets as observed in

EU-1 (**EUO**).³⁹ In short, adsorption capacity measurements of hydrocarbons are consistent with the proposed two-dimensional 10-membered ring channel system in SSZ-58.

4. Conclusions

The synthesis, characterization, and structure solution of the novel high-silica zeolite SSZ-58 have been reported. The structure of SSZ-58 was determined using the ab initio method FOCUS. SSZ-58 possesses a two-dimensional channel system of 10-membered ring pores that intersect to form large cavities circumscribed by elliptical 12- and 16-membered rings. SSZ-58 possesses 12 unique T atoms in its topological structure, making it the most complex structure elucidated from powder data. SSZ-58 and MCM-22 are the only zeolites with two-dimensional channel systems delimited by 10-membered rings. The presence of the 5²4⁵ (D5R) and 5²6⁵ subunits, which have never been observed before, suggests the syntheses of other zeolite topologies with these features are possible.

Electron diffraction and transmission electron microscopy data are consistent with the unit cell determined from indexing of the synchrotron powder data. Rietveld refinement of synchrotron powder X-ray diffraction data in space group *Pm3m* confirms the structural model obtained from the FOCUS method. Argon and hydrocarbon adsorption data strongly support the proposed model. Chemical analyses, TGA measurements, ¹³C NMR experiments, and energy optimizations indicate a high degree of specificity between the 1-butyl-1-cyclooctylpyrrolidinium cation and the cavities positioned at the channel intersections of SSZ-58.

Acknowledgment. This work was supported by the ChevronTexaco Energy Research and Technology Company. Research was carried out in part at the National Synchrotron Light Source, Brookhaven National Laboratory, which is supported by the U.S. Department of Energy, Division of Materials Sciences and Division of Chemical Sciences. We are indebted to S. I. Zones for thoughtful recommendations and careful review of our manuscript. We acknowledge Steve Trumbull for his assistance in the synthesis work. We also thank K. Ong and T. Vogt for their assistance in collecting the synchrotron diffraction data. We are grateful to G. L. Scheuerman, C. R. Wilson, and M. J. Riddle for their support of the new materials research program at ChevronTexaco.

Supporting Information Available: Tables 1S–3S (PDF). This material is available free of charge via the Internet at <http://pubs.acs.org>.

JA021242X

(39) Briscoe, N. A.; Johnson, D. W.; Shannon, M. D.; Kokotailo, G. T.; McCusker, L. B. *Zeolites* **1988**, 8, 74.